MULTI-SENSOR DATA FUSION: PART I

Mark Vaughan[(1)], Yongxiang Hu[(2)], Sharon Rodier[(3)], Tom Arnold[(4)], Dennis Hlavka[(5)]

[(1)] SAIC, MS 475, Langley Research Center, Hampton VA, USA 23681; E-mail: m.a.vaughan@larc.nasa.gov
[(2)] NASA, MS 475, Langley Research Center, Hampton VA, USA 23681; E-mail: Yongxiang.Hu-1@nasa.gov
[(3)] SAIC, MS 927, Langley Research Center, Hampton VA, USA 23681; E-mail: s.d.rodier@larc.nasa.gov
[(4)] SSAI, Goddard Space Flight Center, Code 613.2, Greenbelt, MD USA 20771; E-mail: arnold@climate.gsfc.nasa.gov
[(5)] SSAI, Goddard Space Flight Center, Code 613.1 Greenbelt, MD USA 20771; E-mail: sgdlh@virl.gsfc.nasa.gov

ABSTRACT

We describe a data fusion technique for combining lidar measurements with correlative observations made by passive sensors. Simultaneous measurements obtained by the Cloud Physics Lidar (CPL; [1]) and the MODIS Airborne Simulator (MAS; [2]) serve as inputs to a Kohonen self-organizing map (SOM; [3]) algorithm, which in turn classifies the collocated MAS+CPL pixels according to scene type; i.e., according to the number, the type, and the vertical locations of the cloud and aerosol layers present. Tests conducted using the MAS data alone show that the SOM algorithm recognizes a much greater percentage of the pixels containing high, thin clouds than does the standard MAS cloud mask algorithm. Results obtained when using the combined measurements identify a greater number of distinct classes of data (i.e., scene types) within individual MAS pixels, and thus will allow the selection of more accurate physical models for the retrievals of radiatively significant properties.

1. INTRODUCTION

With the impending (or perhaps now recent) launch of the CALIPSO [4] and CloudSat [5] satellites, remote sensing of the Earth's atmosphere will enter a fundamentally new and different era. When they join the constellation of satellites know as the A-Train [5], the backscatter lidar aboard CALIPSO and the cloud-profiling radar aboard CloudSat will add a new dimension to our understanding of atmospheric composition and dynamics. For the first time, researchers will have access to a global suite of collocated vertical profile measurements to augment the horizontal plane data acquired by existing passive sensors. The potential for scientific discovery engendered by this advance in measurement technology cannot be understated. However, before the promised wealth of A-Train-derived knowledge can be fully realized, a large amount of work must be done in the data analysis arena. Assumptions that once went unchallenged must now be revisited, as their effects on retrieval algorithms must now be considered across a full suite of different sensors. More importantly, the physical model(s) used to retrieve science parameters from the raw data must likewise be consistent for all instruments. In this work we will outline our research in pursuit of realizing this goal. We use CPL and MAS measurements as proxies for the data that will be delivered by their A-Train counter-parts (CALIPSO and MODIS, respectively). Like CALIPSO, CPL provides detailed observations of vertical structure, but is limited to nadir viewing only. MODIS and MAS provide much broader spatial coverage. However, the inversion of the radiometer data is not unique, as it relies on the a priori selection of a physical model that is chosen based on results obtained from scene classification analyses. By combining these two sets of measurements within the framework of the SOM algorithm, we can generate a unified pixel classification scheme informed by the measurements of both instruments. Subsequent, perhaps independent, analyses of the data for both sensors can then employ an identical physical model (or an identical set of assumptions) with regard to the objects being measured. This in turn will enable researchers to make legitimate "apples-to-apples" comparisons using the retrievals derived from lidar and those obtained from passive sensor measurements.

2. SOM OVERVIEW

The Kohonen self-organizing map algorithm belongs to a family of artificial intelligence techniques known as competitive learning (CL). CL clustering makes multiple passes through a data set, and on each pass, the measured data, which is in the form of N time-dependent *feature vectors* $\left(\mathrm{X}(\mathrm{t}) \in \mathbb{R}^{\mathrm{n}}\right)$, is compared to a second, smaller set of template vectors $\left(\mathrm{m}_{\mathrm{i}}(\mathrm{t}) \in \mathbb{R}^{\mathrm{n}}\right)$ that represent cluster centers. For each X_k, a distance metric is applied to determine the specific template, m_c, chosen from among all m_i, that lies closest to the current X_k. The winning template vector is then modified to more closely resemble X_k using a damped learning rule,

$$\mathrm{m}_{\mathrm{c}}(\mathrm{t}+1) = \mathrm{m}_{\mathrm{c}}(\mathrm{t}) + \alpha(\mathrm{t})\left[\mathrm{X}_{\mathrm{k}}(\mathrm{t}) - \mathrm{m}_{\mathrm{c}}(\mathrm{t})\right]. \qquad (1)$$

The quantity $\alpha(t)$ serves as the learning rate, such that $0 < \alpha(t) < 1$, and $\alpha(t)$ is a monotonically decreasing function of t. In the basic CL strategy, only the winning template is modified, and all other template vectors are left unchanged. The SOM algorithm extends the CL algorithm by (a) mapping the multi-dimensional input space into a regularly spaced, two-dimensional grid of nodes, and (b) replacing the simple learning rate, $\alpha(t)$,

with a neighborhood function, $h_{c(x)}(t)$, which allows nodes in the neighborhood of the winning cluster center to also participate in the "learning".

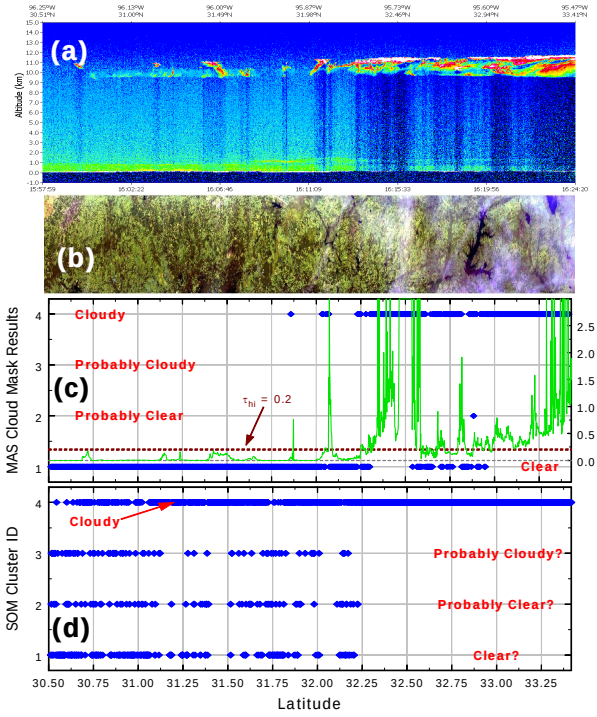

Fig. 1. (a) CPL attenuated backscatter coefficients at 532 nm acquired during the first leg of the 24 November 2002 ER-2 flight; (b) MAS RGB image (channels 20, 10, & 2) acquired coincident with the CPL data; (c) MAS scene classification results (symbols, left axis) for the nadir track pixels; the solid line denotes cirrus cloud optical depths derived from the CPL data; (d) SOM scene classification results for the MAS nadir pixels.

The effectiveness of the SOM algorithm is demonstrated by the four panels shown in Fig. 1. Panel (b) shows a segment of MAS data acquired during the TX-2002 experiment on November 24, 2002. Panel (a) shows the corresponding CPL measurements, which clearly indicate the presence of thin, broken cirrus throughout most of the left hand side of the scene. The bottom two panels show the scene classification results obtained for the nadir pixels of the MAS image. Panel (c) shows the classifications made by the standard MAS/MODIS cloud mask technique [6], while panel (d) shows the results derived using the SOM algorithm. To enable direct comparisons with the MAS results, for this trial the SOM algorithm was configured to identify only four clusters. Both algorithms analyzed the same data. In those regions where the cirrus optical depth exceeds ~0.2 (i.e., on the right-hand side of the scene), the two methods produce nearly identical results. However, in those regions where the cirrus deck is more tenuous ($\tau_{cirrus} < 0.2$), the results returned by the SOM are clearly much more consistent with the coincident CPL measurements. This result may be quite significant, as ice clouds with optical depths of less than 0.2 may play an important role in climate feedback processes. [7] Together with a relatively higher water vapor presence, ice clouds with optical depths of 0.1 at 10km cloud height can trap more than 10 W/m^2 of infrared radiation within the troposphere, and thus significantly warm the planet. The magnitude of potential global warming relies heavily on whether the amount of these thin clouds increases or decreases in response to an increase in greenhouse gases such as CO_2. Yet global observations of these clouds are very poor, precisely because these clouds cannot be effectively identified by passive sensors.

Given the importance of thin cirrus detection, the results shown in Fig. 1 suggest that the SOM would be the technique of choice for scene classifications using MAS and/or MODIS data. That it is not is due to a fundamental difficulty. The physical significance of the SOM output can be very difficult to decipher, and hence the clusters cannot be tagged with meaningful labels. This is illustrated in Table 1, which presents the cluster center statistics for the MAS data used to derive the classifications shown in panel (d) of Fig 1. Based solely on the MAS parameters, there appears to be very little, if any, physical justification for discriminating between clusters 1, 2, and 3. However, as we show below, adding lidar measurements to the feature vectors significantly improves our ability to understand the physical significance of the SOM clusters, and thus allows us to apply meaningful class labels. Furthermore, because the lidar data contains information (e.g., layer heights) not available from MAS, using both sensors also permits reliable identification of more classes of objects.

Table 1: Cluster center values for the classes identified by the SOM analysis of the MAS data shown in Fig 1. Parameters 1 through 3 are MAS reflectances or ratios of MAS reflectances; parameters 4 and 5 are brightness temperatures. The selection criteria for the MAS parameters are given in section 3.

C	0.55 μm	1.6 / 0.55	2.2 / 0.55	12 μm BT	11 μm BT
4	0.066 ± 0.020	1.77 ± 0.31	1.14 ± 0.18	282.1 ± 7.9	283.1 ± 7.2
3	0.049 ± 0.007	2.07 ± 0.18	1.23 ± 0.19	291.2 ± 0.3	291.0 ± 0.3
2	0.052 ± 0.006	2.26 ± 0.21	1.38 ± 0.20	290.8 ± 0.3	291.4 ± 0.3
1	0.054 ± 0.009	2.32 ± 0.23	1.44 ± 0.19	292.2 ± 0.8	292.4 ± 0.8

3. SOM ANALYSES OF SIMULTANEOUS CPL AND MAS MEASUREMENTS

Scene analysis and object classification using data streams derived from multiple instruments requires careful attention to the construction of the feature vectors that will be used by the SOM. The vector elements should be selected to take best advantage of the unique capabilities of each sensor. To reduce the computational complexity in our initial investigations, we characterize the MAS data using only 5 of the 50 available channels. The wavelengths we have selected – 0.55μm,

1.6 μm, 2.2 μm, 11 μm, 12 μm – are sufficient to distinguish between clouds and aerosols, and to differentiate water clouds from ice clouds. Cloudy pixels over water surfaces have higher visible reflectances and lower IR brightness temperatures. Water clouds have larger reflectance ratios between 1.6 μm and 0.55 μm than ice clouds. The 2.2 μm channel provides the land-surface reflectance information required to identify aerosol layers. The brightness temperature differences between the two IR channels aid in the detection of dust layers, and thus provide a further source of information concerning aerosol properties. For the combined MAS+CPL analyses, the CPL measurements are described by an additional nine elements in the feature vector. We derive these by first partitioning the CPL profile into high, middle, and low altitude regimes, using the convention established by the ISCCP [8]. Then, using layer boundaries reported in the standard CPL data products, we compute the integrated attenuated backscatter, γ', for all layers detected in each of the three regions. This calculation is performed separately for the 532 nm channel measurements and the two 1064 nm channels that measure parallel (P) and perpendicular (S) polarization states. By examining the γ' values within each region, we can assess the backscattering intensity (γ'_{532}), understand the general nature of particle shape (via the depolarization ratio, $\delta = \gamma'_{1064S} / \gamma'_{1064P}$), and gain insight into particle size (via the attenuated total color ratio, $\chi' = (\gamma'_{1064S} + \gamma'_{1064P}) / \gamma'_{532}$).

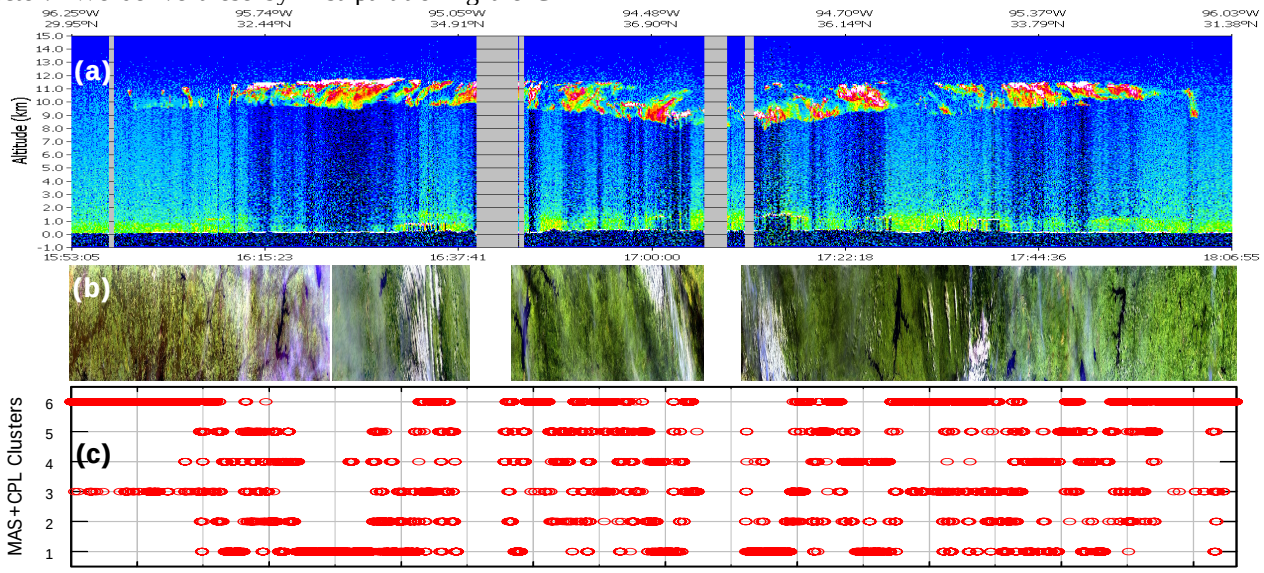

Fig. 2. (a) CPL attenuated backscatter coefficients at 532 nm acquired 24 November 2002; (b) MAS RGB image (channels 20, 10, & 2) acquired coincident with the CPL data; (c) MAS+CPL scene classification results for the nadir track pixels.

Table 2: Cluster center values for the classes identified by the SOM analysis of the MAS+CPL data shown in Fig 2. Parameters 1 through 6 are derived from CPL data; parameters 7 through 11 are derived from MAS data. The "high" and "low" subscripts indicate data derived from, respectively, the high and low altitude regions.

	CPL Parameters						MAS Parameters				
Cluster	γ'_{high}	δ_{high}	χ'_{high}	γ'_{low}	δ_{low}	χ'_{low}	0.55 μm	1.6/0.55	2.2/0.55	12 μm	11 μm
6	0.0031	0.30	0.97	0.0017	0.09	0.83	0.061	2.36	1.52	291.2	291.8
5	0.0097	0.33	0.93	0.0023	0.13	0.78	0.073	2.00	1.38	284.3	285.5
4	0.0165	0.34	0.88	0.0032	0.06	0.73	0.084	1.77	1.26	279.4	280.9
3	0.0038	0.29	0.94	0.0021	0.00	0.80	0.054	1.75	1.10	287.5	288.0
2	0.0086	0.33	0.93	0.0116	0.03	0.85	0.070	1.33	0.98	282.6	283.4
1	0.0217	0.35	0.83	0.0315	0.05	1.00	0.117	1.39	1.07	271.4	273.2

We demonstrate the data fusion capabilities of the SOM above in Fig. 2. In this example we have used all of the data acquired during the 24 November 2002 flight. The CPL measurements for this flight, illustrated in Fig. 2(a), show a highly variable cirrus deck overlying a consistent aerosol layer that in turn contains intermittent low clouds of varying intensity. When present, the cirrus clouds have optical depths that range from sub-visible to in excess of 2. The cirrus alone never totally attenuates the signal. However, there are occasions when the cumulus beneath the cirrus will obscure the surface return. The corresponding MAS measurements are shown in Fig. 2(b). This scene was chosen for our initial data fusion tests because the flight track was entirely over land, and the MAS/MODIS retrieval scheme experiences considerably more difficulty when

analyzing measurements over land surfaces. A further consideration is that the atmospheric data is moderately simple – i.e., we have no mid-level features in this flight track – thus (we hoped!) leading to a more straightforward interpretation of the results.

For our analysis of multi-instrument data, the SOM software was configured to identify six clusters. Because there were no mid-level features in the scene, the feature vectors contained 11 elements. Table 2 presents the mean values for each of these 11 elements and each of the six cluster centers. In contrast to the labeling difficulties encountered when attempting to decipher the previous MAS-only results, the lidar parameters included in the data fusion analysis enable almost instant recognition of different atmospheric objects, and lend themselves to a very straightforward physical interpretation of the six scene types. This can readily be seen by examining the parameters that describe (for example) class 4. The high-altitude parameters indicate moderate cirrus (optical depth of ~0.6), whereas the low-altitude parameters (low γ', low δ, low χ') indicate the presence of aerosol. An excellent example of a class 4 scene is shown in Fig. 2, in the neighborhood of 17:44 GMT. Similarly, class 1 consists of dense cirrus (optical depth of ~1.5) overlying water clouds, which are characterized by high γ', low δ, and high χ'. Representative examples of class 1 scenes occur at ~16:32 GMT and again at ~17:15 GMT. We note, however, that when the cirrus gets especially dense (e.g., at ~16:32 GMT), class 1 can exhibits some classification errors. These can be attributed to renormalization errors that can occur when attempting to correct the backscatter signal beneath the cirrus for the attenuation due to the overlying clouds.

Table 3: Cluster centers for the classes identified by the SOM analysis of the nadir pixels from the MAS data in panel (b) of Fig 2.

C	0.55	1.6 / 0.55	2.2 / 0.55	12	11
6	0.061	2.36	1.52	291.3	291.8
5	0.074	2.07	1.42	284.8	286.1
4	0.083	1.82	1.28	280.2	281.8
3	0.056	1.80	1.14	286.7	287.3
2	0.066	1.25	0.87	282.0	282.8
1	0.128	1.37	1.08	270.6	272.4

For reference, we repeated the SOM analysis using the same nadir-track pixels, and only the MAS components of the feature vectors. The cluster centers for this second experiment are described in Table 3. A qualitative comparison of the MAS parameter means in the two experiments leads to a somewhat surprising (albeit also somewhat tentative) conclusion: apparently, the addition of the lidar data does not greatly influence the cluster centers determined by the SOM. Clearly there is much more information in the MAS/MODIS signal than is generally recognized. However, the SOM-derived classes must be correctly interpreted and accurately labeled if they are to be useful in selecting the physical model used to invert the radiometer data. As shown above, the addition of collocated lidar measurements substantially improves our ability to decipher the physical meaning of the derived classes.

4. CONCLUSIONS & ADDITIONAL WORK

We have described a data fusion technique that synthesizes improved scene classification information from simultaneous lidar and radiometer measurements. While the technique shows promise when applied to radiometer data alone (e.g., as in Fig. 1), difficulties can arise when trying to decipher the physical significance of the clusters that are generated. Including collocated lidar in the analysis eliminates this difficulty, and enables the assignment of physically and linguistically meaningful labels to the clusters.

Our current research focuses on extending the knowledge gained from coincident nadir measurements to the data-rich passive sensor swath. We report the progress we have made in these efforts in a companion paper also published in these proceedings (Rodier, et al.)

REFERENCES

1. M. J. McGill, D. L. Hlavka, W. D. Hart, V. S. Scott, J. D. Spinhirne, and B. Schmid, "The cloud physics lidar: Instrument description and initial measurement results", *Applied Optics*, Vol. 41, 3725– 3734, 2002.
2. King, M. D., Y. J. Kaufman, W. P. Menzel and D. Tanré, "Remote sensing of cloud, aerosol, and water vapor Properties from the Moderate Resolution Imaging Spectrometer (MODIS)", *IEEE Trans. Geosci. Remote Sens.*, Vol. 30, 2–27, 1992.
3. T. Kohonen, *Self-Organization and Associative Memory, 3rd Edition*, Springer-Verlag, Berlin, 2000.
4. D. M. Winker, J. R. Pelon, and M. P. McCormick, "The CALIPSO mission: spaceborne lidar for observation of aerosols and clouds", *Proc. of SPIE*, Vol. 4893, 1–11, 2003.
5. G. L. Stephens and 14 co-authors, "The CloudSat Mission and the A-Train", *Bull. Amer. Meteor. Soc.*, Vol. 83, 1771–1790, 2002.
6. Ackerman, S. A., Strabala, K. I., Menzel, W. P., Frey, R. A., Moeller, C. C., and Gumley, L. E., "Discriminating clear-sky from clouds with MODIS", *Journal of Geophysical Research-Atmospheres*, Vol. 103 (D24), 32141–32157, 1998.
7. Lin, B., B. Wielicki, L. Chambers, Y. Hu, and K-M Xu, "The Iris Hypothesis: A Negative or Positive Cloud Feedback?", *Journal of Climate*, Vol. 15, 3-7, 2002.
8. Rossow, W. B. and R. A. Schiffer, "ISCPP Cloud Data Products", *Bull. Amer. Meteor. Soc.*, Vol. 72, 2–20, 1991.